A Change in the Geodynamics of Continental Growth 3 Billion Years Ago

Bruno Dhuime, *et al.*

Science **335**, 1334 (2012);
DOI: 10.1126/science.1216066

13. T. A. Langdo *et al.*, *Appl. Phys. Lett.* **76**, 3700 (2000).
14. H. Klapper, *Mater. Chem. Phys.* **66**, 101 (2000).
15. J.-S. Park *et al.*, *Appl. Phys. Lett.* **90**, 052113 (2007).
16. J. Bai *et al.*, *Appl. Phys. Lett.* **90**, 101902 (2007).
17. S. Hu, P. W. Leu, A. F. Marshall, P. C. McIntyre, *Nat. Nanotechnol.* **4**, 649 (2009).
18. G. Wang *et al.*, *Appl. Phys. Lett.* **96**, 111903 (2010).
19. E. Feltin *et al.*, *Appl. Phys. Lett.* **79**, 3230 (2001).
20. M. Sakai, T. Egawa, M. Hao, H. Ishikawa, *Jpn. J. Appl. Phys.* **43**, 8019 (2004).
21. Y.-W. Mo, D. E. Savage, B. S. Swartzentruber, M. G. Lagally, *Phys. Rev. Lett.* **65**, 1020 (1990).
22. G. A. Slack, S. F. Bartram, *J. Appl. Phys.* **46**, 89 (1975).
23. Materials and methods and supporting text are available on *Science* Online.
24. C. Rosenblad *et al.*, *J. Vac. Sci. Technol. A* **16**, 2785 (1998).
25. M. Ohtsuka, S. Miyazawa, *J. Appl. Phys.* **64**, 3522 (1988).
26. S. Li, Q. Xiang, D. Wang, K. L. Wang, *J. Cryst. Growth* **157**, 185 (1995).
27. M. Rondanini *et al.*, *J. Appl. Phys.* **104**, 013304 (2008).
28. S. H. Jones, L. K. Seidel, K. M. Lau, M. Harold, *J. Cryst. Growth* **108**, 73 (1991).
29. E. P. Kvam, D. M. Maher, C. J. Humphreys, *J. Mater. Res.* **5**, 1900 (1990).
30. G. R. Booker *et al.*, *J. Cryst. Growth* **45**, 407 (1978).
31. A. Madhukar, *Thin Solid Films* **231**, 8 (1993).

Acknowledgments: Supported by the Swiss federal program funding Nano-Tera through project NEXRAY. Partial support from Fondazione CARIPLO within the MANDIS Project is gratefully acknowledged. We thank Centre Suisse d'Electronique et Microtechnique, Neuchatel, for providing most of the patterned Si substrates used in this work; D. Colombo for preparing the patterned substrates with the submicrometer-wide Si pillars and trenches by means of cryogenic deep reactive ion etching; M. Meduňa for his help in performing and analyzing the synchrotron submicrometer diffraction experiments; B. Batlogg, A. Dommann, A. Neels, R. Kaufmann, A. Pézous, F. Montalenti, F. Pezzoli, E. Bonera, R. Gatti, A. G. Taboada, and T. Kreiliger for valuable discussions; A. Fedorov and K. Mattenberger for technical support; the FIRST Center for Micro- and Nanoscience of ETH Zürich for making available its infrastructure; and the scientific personnel at the ID01 beamline of the European Synchrotron Radiation Facility, Grenoble, in providing user support for the submicrometer diffraction experiments. International patent application WO 2011/135432 has been filed.

Supporting Online Material
www.sciencemag.org/cgi/content/full/335/6074/1330/DC1
Materials and Methods
SOM Text
Figs. S1 to S12
References (*32*–*36*)

8 December 2011; accepted 27 January 2012
10.1126/science.1217666

A Change in the Geodynamics of Continental Growth 3 Billion Years Ago

Bruno Dhuime,[1,2]* Chris J. Hawkesworth,[1] Peter A. Cawood,[1] Craig D. Storey[3]

Models for the growth of continental crust rely on knowing the balance between the generation of new crust and the reworking of old crust throughout Earth's history. The oxygen isotopic composition of zircons, for which uranium-lead and hafnium isotopic data provide age constraints, is a key archive of crustal reworking. We identified systematic variations in hafnium and oxygen isotopes in zircons of different ages that reveal the relative proportions of reworked crust and of new crust through time. Growth of continental crust appears to have been a continuous process, albeit at variable rates. A marked decrease in the rate of crustal growth at ~3 billion years ago may be linked to the onset of subduction-driven plate tectonics.

The timing, rates, and the geodynamical conditions of continental crust generation, destruction, and reworking remain a topic of considerable debate (*1*–*7*). The variations in radiogenic isotope ratios in detrital rocks and minerals are a key archive of the continental record (*3*–*5*, *8*), and the rapid increase in the numbers of U-Pb and Hf isotope analyses of predominantly detrital zircons have provided new constraints for models of crustal evolution (*4*). Hf isotopes in U-Pb–dated zircons are commonly used to characterize the nature of the source of the magma from which the zircon crystallized and to determine the time since this source separated from the upper mantle, commonly referred to as the model age of crust formation (*9*–*11*). However, individual model ages may not represent true periods of crust formation (*12*) because the crustal material analyzed may represent mixtures of older "reworked" and new juvenile material. Continental growth models based simply on U-Pb and Hf isotopes in zircon therefore have a large uncertainty over the proportions of new continental crust generated in different magmatic episodes, and hence over the shape of the continental growth curve (*4*).

Combining stable isotopes, such as oxygen, with the radiogenic isotopes of U-Pb and Lu-Hf (*6*, *13*) may reduce uncertainties surrounding the proportion of new and reworked crust. "Mantle-like" zircons, that is, zircons that crystallized from mantle-derived magmas, have a narrow range of $^{18}O/^{16}O$ (expressed as $\delta^{18}O$ relative to Vienna standard mean ocean water), typically $\delta^{18}O = 5.3 \pm 0.6‰$ (per mil) (2 SD) (*14*). When their parent magmas contain a contribution of sedimentary material or source rocks altered by low- (or high-) temperature hydrothermal activity, the $\delta^{18}O$ in zircons can range to higher (or lower) values (*15*). In principle, periods of juvenile crust formation should be characterized by zircons with mantle-like $\delta^{18}O$ and similar radiogenic Hf model ages (*6*). Conversely, periods dominated by crustal reworking result in the generation of "supracrustal" zircons, typically with elevated $\delta^{18}O$ values and varying Hf model ages (*13*, *15*, *16*). To the extent that Hf isotope ratios of supracrustal zircons represent mixtures, they will not record true periods of crustal growth (*6*). There are relatively few studies in which U-Pb and Hf isotopes are combined with O isotopes in zircon (*6*, *7*, *17*, *18*), and evaluating crustal growth models based on large data sets of zircons remains difficult, especially when constraining the proportions of new crust formation ages to those that are arguably hybrid ages (*4*, *8*, *19*).

$\delta^{18}O$ values are plotted as a function of Hf model ages in 1376 detrital and inherited zircons from Australia, Eurasia, North America, and South America (Fig. 1A) (*11*). These data are taken to be representative of the Hf-O isotope record available for Earth's continental crust. Overall supracrustal zircons with Meso/Paleo-Proterozoic Hf model ages show a greater range of $\delta^{18}O$ values than those with older or younger model ages, and they are more abundant than mantle-like zircons. The proportions of mantle-like zircons and supracrustal zircons in turn determines the relative proportions of new crust formation ages and hybrid model ages induced by crustal reworking processes in the distribution of Hf model ages (Fig. 1B). The proportion of new crust formation ages does not change substantially in the first billion years of Earth's history, with a median value ~73%. From ~3.2 billion years ago (Ga), the proportion of new crust formation ages gradually decreases down to ~20% at ~2 Ga, and it then increases to ~100% toward the present day (Fig. 1B). Assuming that these observations characterize the continental crust as a whole, this parameterization allows us to predict the proportion of new crust and hybrid model ages throughout Earth's evolution and, hence, access the large U-Pb and Hf isotope data sets that do not include $\delta^{18}O$ data (*4*, *8*, *19*).

Young sediments typically contain zircons with a wide range of ages, so they appear to provide records that are more representative of the magmatic history of the crust than zircons in igneous rocks or in old sediments (*5*). A compilation of 6972 analyses of detrital zircons with deposition ages ranging from the late Paleozoic to the present day (*11*) results in a distribution of Hf model ages that does not simply reflect the generation of new crust, because it still includes

[1]Department of Earth Sciences, University of St. Andrews, North Street, St. Andrews KY16 9AL, UK. [2]Department of Earth Sciences, University of Bristol, Wills Memorial Building, Queens Road, Bristol BS8 1RJ, UK. [3]School of Earth and Environmental Sciences, University of Portsmouth, Burnaby Road, Portsmouth PO1 3QL, UK.

*To whom correspondence should be addressed. E-mail: b.dhuime@bristol.ac.uk

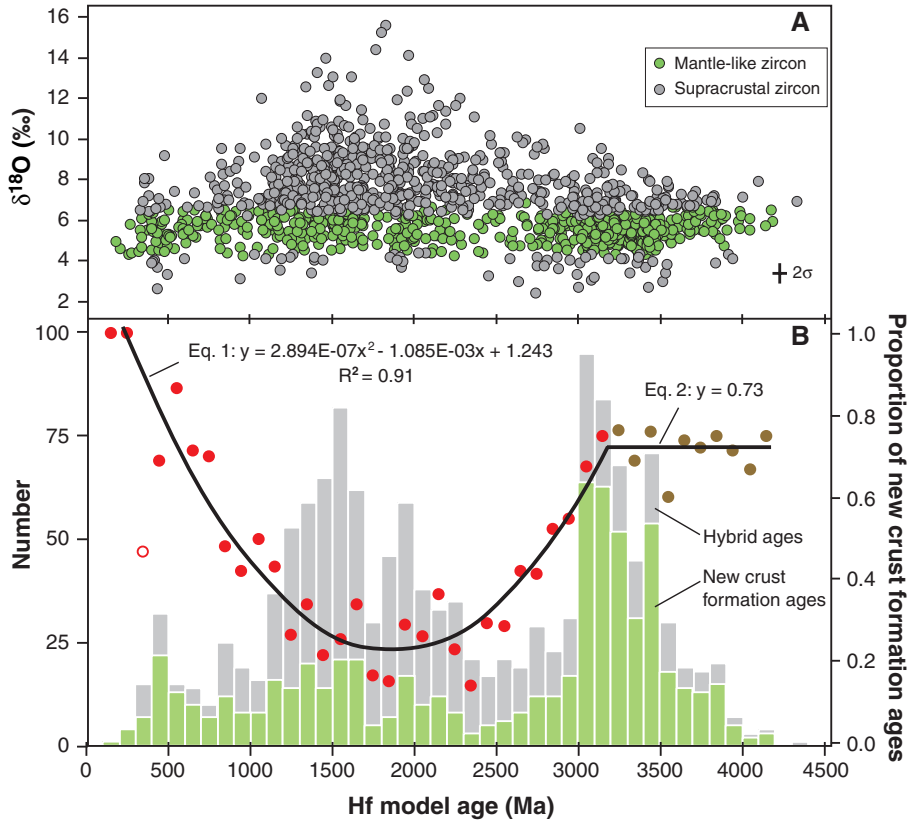

Fig. 1. (**A**) $\delta^{18}O$ versus Hf model ages in 1376 detrital and inherited zircons (*11*) from Australia [this study, $n = 458$; and (*6*), $n = 106$], Eurasia (*18*, *29*) ($n = 488$), North America (*7*, *17*) ($n = 232$), and South America (*30*) ($n = 92$). Zircons with $\delta^{18}O$ within error of the mantle-like zircons domain [$\delta^{18}O = 5.3 \pm 0.6‰$, 2 SD (*14*)] are referred to as mantle-like zircons. Their Hf model ages record periods when new crust is generated. Other zircons are referred to as supracrustal. Their Hf model ages are referred to as "hybrid," because they may not record true periods of new crust formation. Model ages are calculated using the reference line for the Hf isotope evolution of the new crust of (*9*) and $^{176}Lu/^{177}Hf = 0.015$ for the crustal source. The calculated model ages are sensitive to the values chosen, but the shape of the age distributions are much less so (figs. S1 and S2). (**B**) O isotopes are used to distinguish hybrid model ages (grey bins, supracrustal zircons data) from model ages that represent periods of new crust generation (green bins, mantle-like zircon data). The data points represent the proportion of Hf model ages associated with new crust generation in the worldwide zircon record, calculated for 100-million-year time intervals, and when there are $n \geq 3$ analyses for each time interval. The red and brown dots define a relationship through time (black curve) that is defined by Eqs. 1 and 2, respectively (the white-filled red dot was not included in the calculation of Eq. 1).

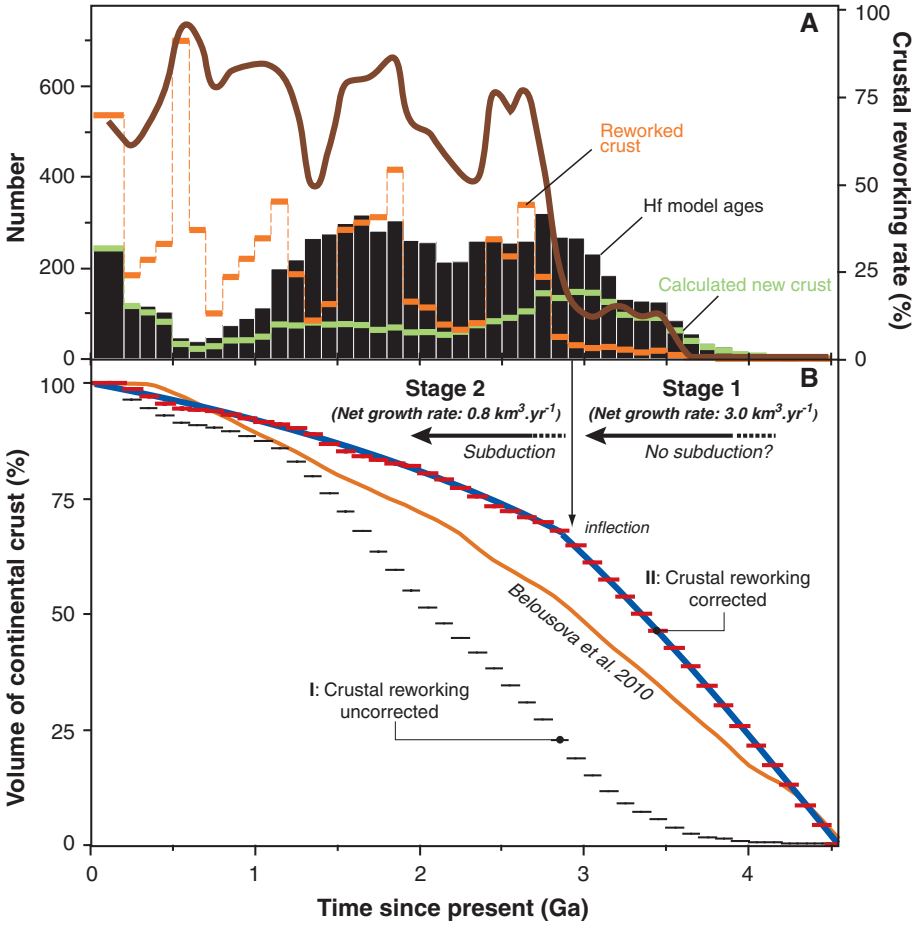

Fig. 2. (**A**) Distribution of the Hf model ages, calculated new crust ages, and reworked crust ages through time, from a worldwide database of 6972 U-Pb and Hf analyses of zircons from young sediments, with deposition ages ranging from the late Paleozoic to the present day (*11*). All calculations are presented for every 100-million-year time interval starting from 200 million years ago (Ma). The youngest bin is for 200 Ma because of uncertainty over the range of deposition ages of the sediments. The brown curve represents the variation in the rates of reworking of the continental crust through time, calculated from the distributions of the proportions of reworked crust (orange histogram) and new crust (green histogram). (**B**) Continental growth curves calculated from the same database as (A). The cumulative volume of crust is calculated for 100-million-year time intervals. Curve I (black) is calculated from the cumulative proportions of the Hf model ages through time [black histogram in (A)]. Curve II (red) integrates the variations of the reworking rates [brown curve in (A)] in the calculations of the cumulative proportions of the newly formed crust through time. The blue curve highlights the main variations observed in curve II. The overall shape of this curve is not substantially affected by the selection of the Lu/Hf ratios in the crust and the Hf isotope ratios of new continental crust in the calculation of individual model ages (figs. S1 and S2). The curve obtained by Belousova *et al.* (*4*) from a U-Pb-Hf database of 13,844 zircons of various ages and origin is reported for comparison.

hybrid model ages (Fig. 2A). However, using these data, and our relation that characterizes the proportion of new crust and hybrid model ages through time (Fig. 1B, Eqs. 1 and 2), we were able to calculate the distribution of new crust formation ages (Fig. 2A).

The net volume of new continental crust generated during magmatic episodes depends on the variations in the proportion of newly formed and reworked crust that is preserved through time. A broader proxy for the variations of the reworked crust through time is given by the distribution of the crystallization ages of zircons with Hf model ages greater than their crystallization ages (Fig. 2A). These variations may be linked to times of supercontinent assembly, periods that are characterized by both increased crustal reworking and preservational bias (*8*, *20*, *21*). The variation in the rates of crustal reworking through time, which is given by the variations in the proportions of the reworked crust versus calculated new crust, reveals low crustal reworking rates (< 20%) from the Hadean to the Meso-Archean. A rapid increase to around 75% reworking is observed at ~3 Ga, and then relatively high reworking rates (>50%) are observed until the present day.

This parameterization has several implications for models of the rates of growth of the continental crust (Fig. 2B). The distribution of Hf model ages, irrespective of their oxygen isotope ratios and the extent to which they include hybrid model ages (Fig. 2A), provides an estimate of the minimum volume of the preserved continental crust that was present through time, because it does not integrate the variations in the proportions of reworked and new crust. If, however, the model integrates crustal generation and reworking rates (Fig. 2A), we see that ~65% of the present-day volume of the crust was established by 3 Ga (Fig. 2B) and that there was a sharp change in the net rates of growth of the continental crust at that time. These features are not observed in continental growth curves calculated from large U-Pb and Hf in zircon databases in the absence of O isotope data (*4*).

Based on this analysis, we propose a two-stage model for continental growth (Fig. 2B). Stage 1 (>4 Ga to ~3 Ga) is characterized by relatively high net rates of continental growth. Given the present-day volume of the continental crust of 7.10^9 km^3 [e.g., (*22*)], the average net rate of growth of the continental crust for Stage 1 was ~3.0 km^3 year^{-1}. This is similar to the rates at which new crust is generated and destroyed at the present time (*22*, *23*). The average net growth rate for Stage 2 (~3 Ga to the present day) is ~0.8 km^3 year^{-1}, and the inflection in the rate of crustal growth curve at ~3 Ga indicates a fundamental change in the way the continental crust was generated and preserved. The difference in the net rates of crustal growth in Stages 1 and 2 can be accommodated by high rates of destruction of continental crust in Stage 2 compared with Stage 1 (Fig. 2A). The inferred high crustal destruction rates in Stage 2 strongly suggest that it reflects the onset of subduction-driven plate tectonics and discrete subduction zones at ~3 Ga, consistent with independent arguments from recent studies (*24*–*26*). Geodynamical processes that might have dominated in Stage 1 include shallow subduction and delamination (*27*) or "intraplate" lithospheric extension/mantle upwelling (*26*, *28*), both of which could produce crust at rates similar to today (~3.0 km^3 year^{-1}).

References and Notes

1. K. C. Condie, *Earth Planet. Sci. Lett.* **163**, 97 (1998).
2. B. Dhuime, C. J. Hawkesworth, C. D. Storey, P. A. Cawood, *Geology* **39**, 407 (2011).
3. C. J. Allègre, D. Rousseau, *Earth Planet. Sci. Lett.* **67**, 19 (1984).
4. E. A. Belousova *et al.*, *Lithos* **119**, 457 (2010).
5. C. J. Hawkesworth *et al.*, *J. Geol. Soc. London* **167**, 229 (2010).
6. A. I. S. Kemp, C. J. Hawkesworth, B. A. Paterson, P. D. Kinny, *Nature* **439**, 580 (2006).
7. C. Y. Wang, I. H. Campbell, C. M. Allen, I. S. Williams, S. M. Eggins, *Geochim. Cosmochim. Acta* **73**, 712 (2009).
8. K. C. Condie, M. E. Bickford, R. C. Aster, E. Belousova, D. W. Scholl, *Geol. Soc. Am. Bull.* **123**, 951 (2011).
9. B. Dhuime, C. J. Hawkesworth, P. A. Cawood, *Science* **331**, 154 (2011).
10. D. J. DePaolo, *Nature* **291**, 193 (1981).
11. Materials and methods are available as supporting material on *Science* Online.
12. N. T. Arndt, S. L. Goldstein, *Geology* **15**, 893 (1987).
13. C. J. Hawkesworth, A. I. S. Kemp, *Chem. Geol.* **226**, 144 (2006).
14. J. W. Valley, P. D. Kinny, D. J. Schulze, M. J. Spicuzza, *Contrib. Mineral. Petrol.* **133**, 1 (1998).
15. J. W. Valley *et al.*, *Contrib. Mineral. Petrol.* **150**, 561 (2005).
16. A. I. S. Kemp *et al.*, *Science* **315**, 980 (2007).
17. A. B. Pietranik *et al.*, *Geology* **36**, 875 (2008).
18. C. Y. Wang, I. H. Campbell, A. S. Stepanov, C. M. Allen, I. N. Burtsev, *Geochim. Cosmochim. Acta* **75**, 1308 (2011).
19. P. J. Voice, M. Kowalewski, K. A. Eriksson, *J. Geol.* **119**, 109 (2011).
20. I. H. Campbell, C. M. Allen, *Nat. Geosci.* **1**, 554 (2008).
21. C. J. Hawkesworth, P. A. Cawood, T. Kemp, C. Storey, B. Dhuime, *Science* **323**, 49 (2009).
22. D. W. Scholl, R. von Huene, in *Earth Accretionary Systems in Space and Time,* P. A. Cawood, A. Kröner, Eds. (Geological Society, London, Special Publications, 2009), vol. 318, pp. 105–125.
23. D. W. Scholl, R. von Huene, in *4-D Framework of Continental Crust,* R. D. Hatcher, M. P. Carlson, J. H. McBride, J. R. M. Catalán, Eds. (Geological Society of America Memoir, 2007), vol. 200, pp. 9–32.
24. P. A. Cawood, A. Kröner, S. Pisarevsky, *GSA Today* **16**, 4 (2006).
25. S. B. Shirey, S. H. Richardson, *Science* **333**, 434 (2011).
26. M. J. Van Kranendonk, *Science* **333**, 413 (2011).
27. S. F. Foley, S. Buhre, D. E. Jacob, *Nature* **421**, 249 (2003).
28. M. J. Van Kranendonk, *Am. J. Sci.* **310**, 1187 (2010).
29. P. J. Lancaster, C. D. Storey, C. J. Hawkesworth, B. Dhuime, *Earth Planet. Sci. Lett.* **305**, 405 (2011).
30. C. W. Rapela *et al.*, *Gondwana Res.* **20**, 673 (2011).

Acknowledgments: This work was supported by the Natural Environment Research Council (NERC, NE/E005225/1) and the University of St. Andrews. The data reported in this paper are archived in the supporting online material. We are grateful to staff members of Edinburgh Ion Microprobe Facility (EIMF) for technical assistance with oxygen isotope analysis. The comments of the anonymous referees and the discussions with T. Kemp and T. Elliott during the revision of this article have been greatly appreciated.

Supporting Online Material

www.sciencemag.org/cgi/content/full/335/6074/1334/DC1
Materials and Methods
SOM Text
Figs. S1 and S2
References (*31*–*72*)

1 November 2011; accepted 9 February 2012
10.1126/science.1216066

The Multielectron Ionization Dynamics Underlying Attosecond Strong-Field Spectroscopies

Andrey E. Boguslavskiy,[1]* Jochen Mikosch,[1]* Arjan Gijsbertsen,[1,2]* Michael Spanner,[1] Serguei Patchkovskii,[1] Niklas Gador,[3] Marc J. J. Vrakking,[2,4] Albert Stolow[1]†

Subcycle strong-field ionization (SFI) underlies many emerging spectroscopic probes of atomic or molecular attosecond electronic dynamics. Extending methods such as attosecond high harmonic generation spectroscopy to complex polyatomic molecules requires an understanding of multielectronic excitations, already hinted at by theoretical modeling of experiments on atoms, diatomics, and triatomics. Here, we present a direct method which, independent of theory, experimentally probes the participation of multiple electronic continua in the SFI dynamics of polyatomic molecules. We use saturated (*n*-butane) and unsaturated (1,3-butadiene) linear hydrocarbons to show how subcycle SFI of polyatomics can be directly resolved into its distinct electronic-continuum channels by above-threshold ionization photoelectron spectroscopy. Our approach makes use of photoelectron-photofragment coincidences, suiting broad classes of polyatomic molecules.

To date, measurements of attosecond electronic dynamics in atoms and molecules (*1*) have typically involved strong laser-field processes. Even pump-probe spectroscopies using isolated attosecond pulses rely on the presence of a phased, strong (~10^{13} W/cm^2) laser field (*2*–*4*). The process of high harmonic generation (HHG), which can probe electronic wave packets on attosecond time scales (*5*–*9*), is entirely based on strong-field ionization (SFI), as is the use of subcycle electron recollision for probing dynamics (*10*, *11*). In the interpretation of experiments, broad use is made of the three-step model (*12*) wherein SFI adiabatically releases, via